New Spectroscopic Insight into the Deactivation of a ZSM-5 Methanol-to-Hydrocarbons Catalyst

Andrea Zachariou,[a, b] Alexander P. Hawkins,[a, b] Suwardiyanto,[c] Paul Collier,[d] Nathan Barrow,[d] Russell F. Howe,[e] Stewart F. Parker,*[a, b, f] and David Lennon[a]

The nature of the hydrocarbon pool at different stages of the methanol-to-hydrocarbons reaction over ZSM-5 is examined. A combination of reaction testing, analytical and spectroscopic techniques is employed to investigate changes in the nature and form of the hydrocarbon pool as a function of reaction conditions and reaction time. It is shown that inelastic neutron scattering spectroscopy (INS) complements other spectroscopic methods for observing molecular components in the hydrocarbon pool of working catalysts. INS is uniquely able to spectroscopically identify the form of coke species present in deactivated catalysts.

Introduction

The methanol-to-hydrocarbons (MTH) reaction over an acidic zeolite catalyst such as ZSM-5 is an important class of reaction to produce olefins and methylated aromatics, with the reaction thought to proceed by a 'hydrocarbon pool' (HCP) mechanism. Here, two catalytic cycles (olefinic and aromatic) work in tandem involving processes such as hydrogen transfer, methylation, cyclisation, cracking and dealkylation to ultimately lead to a mixture of commercially valuable hydrocarbons.[1–6]

Alongside conventional reaction testing (*e.g.*, micro-reactor), a wide range of analytical probes have been employed to investigate MTH chemistry over ZSM-5, with solid-state NMR spectroscopy providing particular insight.[1,2] FTIR studies have identified the first stages of carbon-carbon bond formation and the early evolution of the HCP,[7–14] but are not suited to studying the deactivation stages of the MTH reaction. Raman techniques have been employed in studying the evolution of coke build up, however, Raman spectra contain fluorescent emission due to the presence of polycyclic aromatic molecules.[15–17] UV-Raman[15,16] and Kerr gated Raman[17] techniques have been successfully used as alternatives in order to suppress fluorescence, but sample degradation is still a problem due to the high intensity laser powers employed. UV-VIS spectroscopy has been used extensively to identify individual components of the HCP, but interpretation of the broad overlapping bands can be problematical, particularly at longer reaction times.[14,18–27] NMR spectroscopy is highly successful at providing insight in the initial and steady state stages. However, it has difficulties identifying deactivating species at longer reaction times due to the reduced hydrogen content and preponderance of spinning side bands.[28–36]

One technique that is providing a fresh perspective to issues in contemporary industrial heterogeneous catalysis is that of inelastic neutron scattering (INS). The technique possess novelty in that it can provide access to a wide vibrational spectral range (20–4000 cm^{-1} in favourable circumstances) with hydrogenous modes dominating the spectra.[37,38] In this way, the zeolite framework makes minimal contribution to the spectrum but the vibrational modes of reagent, intermediates and products retained at the catalyst surface are observable. Moreover, mode intensity and vibrational frequency are amenable to simulation via DFT methods; a fact that significantly aids vibrational assignment.[38] Howe and co-workers have recently reviewed neutron spectroscopy studies of MTH catalysis over ZSM-5.[39] Importantly, that work highlights the ability of INS to interrogate technical catalyst samples without the need for any

[a] *A. Zachariou, A. P. Hawkins, Dr. S. F. Parker, Prof. D. Lennon*
School of Chemistry
University of Glasgow
Joseph Black Building
Glasgow, G12 8QQ (UK)
[b] *A. Zachariou, A. P. Hawkins, Dr. S. F. Parker*
UK Catalysis Hub
Research Complex at Harwell
STFC Rutherford Appleton Laboratory
Chilton, Oxon, OX11 0FA (UK)
[c] *Dr. Suwardiyanto*
Department of Chemistry
University of Jember
Jember 68121 East Java (Indonesia)
[d] *Dr. P. Collier, Dr. N. Barrow*
Johnson Matthey Plc.
Johnson Matthey Technology Centre
Blounts Court
Sonning Common
Reading, RG4 9NH (UK)
[e] *Prof. R. F. Howe*
Department of Chemistry
University of Aberdeen
Meston Building
Aberdeen, AB24 3UE (UK)
[f] *Dr. S. F. Parker*
ISIS Neutron and Muon Source
ISIS Facility
STFC Rutherford Appleton Laboratory
Chilton, Oxon, OX11 0QX (UK)
E-mail: stewart.parker@stfc.ac.uk

Supporting information for this article is available on the WWW under https://doi.org/10.1002/cctc.202100286

subsequent sample preparation or treatment, including deactivated samples. Deactivation in heterogeneous catalysis is an important issue[40] but one that is not always amenable to investigation by molecular spectroscopy. For example, via several processes such as carbon retention, sintering, oligomer formation, *etc.*, zeolite catalysts tend to darken on ageing. Thus, for samples that have experienced extended periods of time-on-stream, analysis by infrared spectroscopy or UV-VIS spectroscopy is unproductive due to total absorption by the substrate.[40] INS is not influenced at all by the colour of the sample.

This article concentrates on using INS to characterise different stages of the catalyst lifetime for a ZSM-5 catalyst applied to MTH chemistry, supported by other forms of spectroscopy. Crucially, the matter of the molecularity of the hydrocarbon pool as the catalyst approaches a deactivation regime is examined. Schulz *et al.* report on how temperature plays a role in changing the deactivation mechanism of the MTH reaction.[41] Reaction temperatures below 350 °C are associated with a build-up of methylated and polycyclic aromatics within the zeolite pores, causing pore blockage and deactivating the catalyst from the inside out. However, reaction in the range 350–500 °C showed the deactivation mechanism to have significantly altered, with graphitic coke building up rapidly on the external surface of the zeolite.[41] This temperature dependent behaviour was also observed by Borodina *et al.*, in their UV-Vis studies of coke formation in SSZ-13.[18] XPS studies by Sexton *et al.* showed that external coke formed only after deactivation of the catalyst at 370 °C.[42] Mores *et al.* suggest that the carbonaceous build-up occurs more rapidly where the straight channels of the zeolite reached the external surface, with two types of coke being identified.[19,43] Building on this platform, here we investigate MTH surface chemistry at three different reaction temperatures: (i) 300 °C, indicative of internal carbon build-up of the zeolite catalyst,[40] (ii) 350 °C for steady-state operation,[2,5,44] and (iii) 400 °C where deactivation by carbon deposition proceeds externally first, before moving in to the bulk.[41] The study is further complemented by additionally studying two temporal windows. Firstly, a time-on-stream (T-o-S) of *ca.* 2 h emphasizes preliminary reactions in the catalytic cycle and, secondly, T-o-S $\geq$ 40 h samples steady-state and quasi-deactivation regimes. No constant T-o-S was used for the second class of reactions; the reaction times of 40–110 h are selected as being representative of extended catalytic turnover. Vibrational assignments make use of a recently published report on the INS spectra of a variety of unsaturated hydrocarbons that constitute candidate species for contributors to the pivotal HCP.[45]

The sample sizes of the INS experiments are much larger than the laboratory scale samples used for other spectroscopies. This is due to the relative insensitivity of INS. However, the sample size requirement allows for reaction testing to be completed on a larger scale as well, which is between laboratory scale samples and industrial samples. There is a gap in literature pertaining to the study of large-scale samples, and how the change in sample size could affect the MTH reaction.

Results and Discussion

Reaction testing

Reaction testing was undertaken at 300, 350 and 400 °C using two reactor configurations. Firstly, a conventional micro-reactor (catalyst charge ~500 mg) was used to determine reaction trends, whilst secondly a larger scale reactor (catalyst charge ~12 g) was used to prepare samples for INS analysis. Due to the relatively insensitive nature of INS spectroscopy, the technique requires relatively large sample masses, which leads to distinct sample environment arrangements as considered elsewhere.[46] Table S1 in the ESI outlines the reaction conditions employed, producing a series of six samples. Table 1 presents physical characterisation of those samples post-reaction. Figure S1 (ESI) shows GC analysis of the microreactor data that is consistent with previous reports of ZSM-5/MTH chemistry.[1,2,47,48]

For the INS reactor, Figure S2 shows in-line mass spectrometry profiles that sample the reactor exit stream vapour phase, whilst Figure S3 presents GC-MS analysis of material periodically sampled from a catch-pot that collects higher molecular weight condensable products. Figures S2 and S3 show the product distribution of the INS reactor to be comprised of light olefins and low molecular weight methylated aromatics. Figure 1 shows the methanol conversion profiles for three different temperatures performed in the INS reactor. Initially all samples exhibit high methanol conversion, but this progressively declines on increasing T-o-S. The 300 and 350 °C runs follow similar trajectories but the steeper decline for the 400 °C sample indicates this sample to be more rapidly approaching a deactivation phase. Taken together, this sequence of reaction test data (Figure 1, Figures S1–S3) is comparable with previously published ZSM-5 MTH performance.[2,47,48]

Post-reaction samples from the INS reactor have undergone extensive characterisation, with the results presented in the Supporting Information section (Figures S4–S16). Briefly, Figure S4 shows the temperature-programmed oxidation profiles of the short run catalyst samples (2 h) to possess two types of coke (Type I and Type-II),[41,49] with a large proportion of the coke attributed to light hydrocarbons with a high H/C ratio.[50] For longer reaction times, there is an increase in the population of aromatic and polycyclic hydrocarbons as well as evidence of

Table 1. Nitrogen adsorption data and coke content for the fresh, unreacted catalyst and six post-reaction samples prepared using the INS reactor.

Sample Name[a]	S_{BET} [$m^2 g^{-1}$]	$V_{micropore}$ [$cm^3 g^{-1}$]	$S_{external}$ [$m^2 g^{-1}$]	Coke content [wt%]
Unreacted ZSM-5	370	0.172	37	N/A
300–2 h	371	0.140	35	1.95
350–2 h	397	0.150	36	2.58
400–2 h	368	0.139	42	2.46
300–60 h	56	0.016	18	8.97
350–110 h	46	0.014	13	14.20
400–44 h	38	0.011	12	20.20

[a] The sample coding is as follows: the number preceding the hyphen signifies the reaction temperature (°C), whilst the number after the hyphen signifies the reaction time (h).

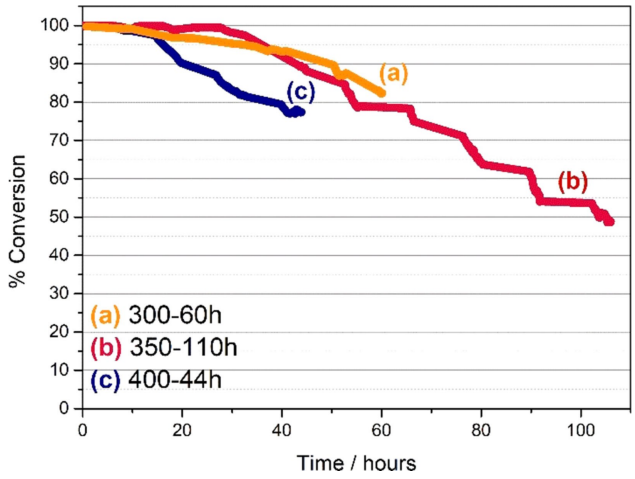

Figure 1. Methanol conversion for MTH reactions carried out in the INS reactor at three different temperatures: (a) 300, (b) 350 and (c) 400 °C.

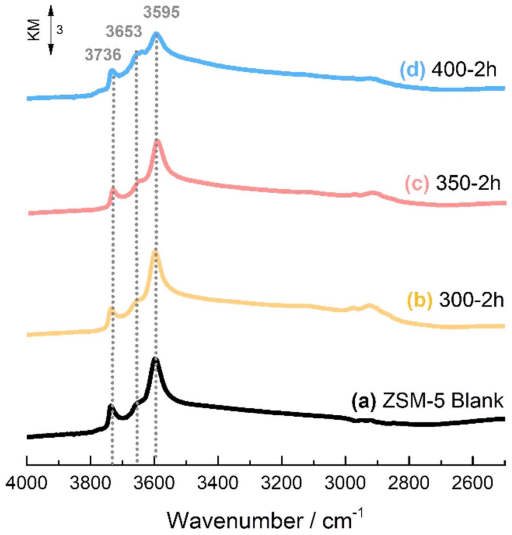

Figure 2. Stacked DRIFTS spectra (4000–2500 cm^{-1}) of the ZSM-5 catalyst post-reaction after 2 h T-o-S at the following reaction temperatures: (b) 300, (c) 350 and (d) 400 °C. The spectra were recorded at the reaction temperatures, and normalised on the zeolite overtone at 1876 cm^{-1}. Spectrum (a) corresponds to an activated but unreacted sample of ZSM-5 recorded at 350 °C. The size bar indicates spectral intensity in Kubelka-Munk units for each spectrum.

graphitic carbon. Graphite formation at the catalyst surface is most noticeably evident for the 400–44 h sample.

Table 1 shows the coke percentage values obtained from the TPO analysis (and confirmed via TGA) as well as the nitrogen adsorption data. On comparing the short runs, increasing reaction temperature does not unduly affect surface area or micropore volume, nor does it induce major differences in the coke content. However, in contrast, Table 1 shows the samples that have experienced extended T-o-S to exhibit decreases in internal surface area, external surface area and micropore volume. Bibby *et al.* reported that 14–18 wt% coke content is typical for deactivated catalysts used in MTH chemistry.[50] Unsurprisingly, the 400–44 h sample displays the highest coke content, with the extent indicative of operation within a deactivation or quasi-deactivation regime.

Diffuse-reflectance infrared Fourier transform spectroscopy (DRIFTS)

Figure 2 presents a stack plot of diffuse-reflectance infrared spectra (DRIFTS) of the ZSM-5 catalyst after 2 h T-o-S as a function of reaction temperature over the energy range 2500–4000 cm^{-1}; the region below 2200 cm^{-1} being obscured by strong absorption of framework bands (see below). Figure 2(a) shows the unreacted ZSM-5 to exhibit three major OH environments: (i) Brønsted acid sites (3595 cm^{-1}); (ii) extra-framework aluminium (Al–OH) (3653 cm^{-1}); (iii) silanol groups located at the external surface of the zeolite (3736 cm^{-1}).[47,51,52] Upon reaction Figure 2(b–d) show that increasing temperature progressively diminishes the intensity of the Brønsted acid sites, whilst there is a relative increase in the Al–OH band intensity; this scenario is suggestive of hydrolysis of the acid sites at elevated temperatures. Wide-scan DRIFTS spectra for the extended run samples are presented in Figure 3, where the spectra have been normalised with respect to the 1876 cm^{-1} overtone band of the zeolite framework. This format is selected

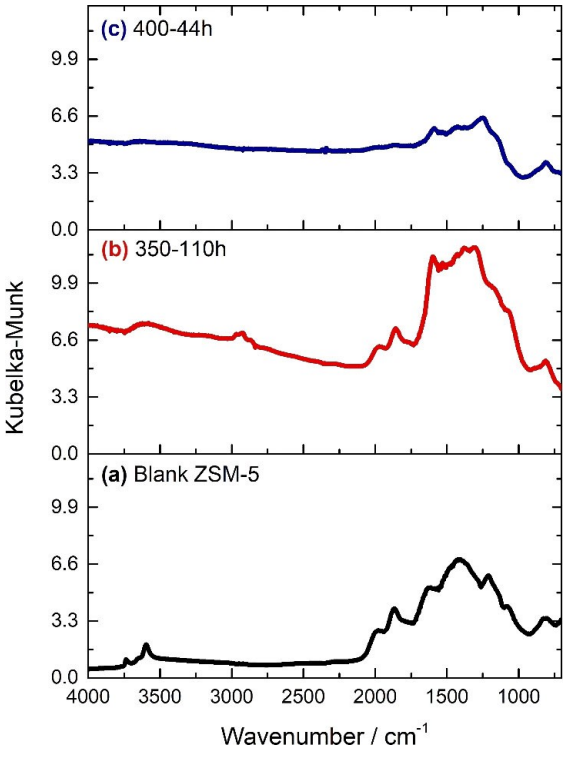

Figure 3. DRIFTS spectra (4000–500 cm^{-1}) of the ZSM-5 catalyst post-reaction after extended T-o-S at the following reaction temperatures: (b) 350–110 h and (c) 400–44 h. The spectra were recorded at their reaction temperature. Spectrum (a) corresponds to an activated, but unreacted, sample of ZSM-5 recorded at 350 °C.

on this occasion to illustrate difficulties that may be encountered when using infrared spectroscopy to examine heterogeneous catalysts for extended periods of T-o-S.[39]

Compared to Figure 3(a), significant broadening of the OH region is observed in Figure 3(b–c), making it difficult to distinguish the different OH environments. This loss of spectral identity in the diagnostic 4000–2500 cm^{-1} region of the spectrum could arise from two factors: (i) a loss of Brønsted acid sites and/or (ii) a loss of diffuse reflectivity due to the sample colour becoming progressively darker at the longer reaction times. Although the ν(C–H) modes of the HCP are visible for the 350 °C spectrum (Figure 3b), with the peaks resembling the coke bands seen for catalysts previously used for methanol conversion at 350 °C over three days,[47] there is an almost complete loss of diffuse reflectivity for the 400 °C sample (Figure 3(c). Indeed, it is possible that (i) and (ii) could be coincident events: Table 1 (Section 2.1) shows the long-run 400 °C sample to possess the highest coke content and neither ν(C–H) or ν(O–H) modes are detectable in Figure 3(c). Moreover, the fact that Figure 3 shows a progressive increase in the baseline of the infrared spectrum for increasing reaction temperature (signifying greater advancement of the reaction coordinate) illustrates a limitation of IR spectroscopy to characterise and interrogate certain aged heterogeneous catalysts. Against this background, it was deemed profitable to employ the technique of inelastic neutron scattering (INS) spectroscopy to access the vibrational spectrum of aged MTH catalysts.

INS spectroscopy

Figure S6 presents the INS spectra for the post-reaction short run samples. The spectra are of low intensity indicating relatively little hydrogenous material to be present, as expected from the coke content (Table 1). The lack of definition of the bands indicates an absence of discrete molecular entities; rather, the profile is consistent with a mixture of species. In this way, Figure S6 shows that the hydrocarbon pool is not fully developed after T-o-S = 2 h.

The INS spectra for the long-run samples that correspond to steady-state and quasi-deactivation regimes are presented in Figure 4. In contrast to the short run spectra, well-defined INS spectra are observed. Two different INS spectrometers were used to obtain spectra in the range 20–4000 cm^{-1} at favourable resolution. Figure 4(a) presents spectra in the range 0–2000 cm^{-1} that were recorded using the TOSCA spectrometer,[37,53,54] whereas, Figure 4(b) shows the spectral response over the energy range 2000–4000 cm^{-1} that was recorded using the MAPS spectrometer.[37,55] Figure 4 defines the vibrational fingerprint of the hydrocarbon pool (HCP) for the extended duration variable temperature runs. To the best knowledge of the authors, this is the first time that vibrational spectra of this specification (energy range and resolution) for MTH catalysts operative over such a wide range of conditions have been reported. The spectra for the 300 (i) and 350 °C (ii) runs in Figure 4(a) are comparable and exhibit a similar pattern to previously reported ZSM-5/MTH HCP INS spectra.[47,56,57] The general profile observed for both samples also closely resembles the spectrum of ZSM-5 upon exposure to dimethyl ether at elevated temperatures.[56] From the variety of spectral features present in Figure 4(a)(i and ii), no single molecular entity is deemed to be present; the spectra represent a mixture of hydrocarbon species. Figure 4(a)(iii) shows significant changes on progressing to the 400 °C sample. As considered in Section 2.1, the 400–44 h sample has experienced a higher degree of deactivation; inspection of Figure 4(a)(iii) shows that this has altered the composition and form of the hydrocarbonaceous entities retained within the porous network of the zeolite, *i.e.*, the all-important HCP.

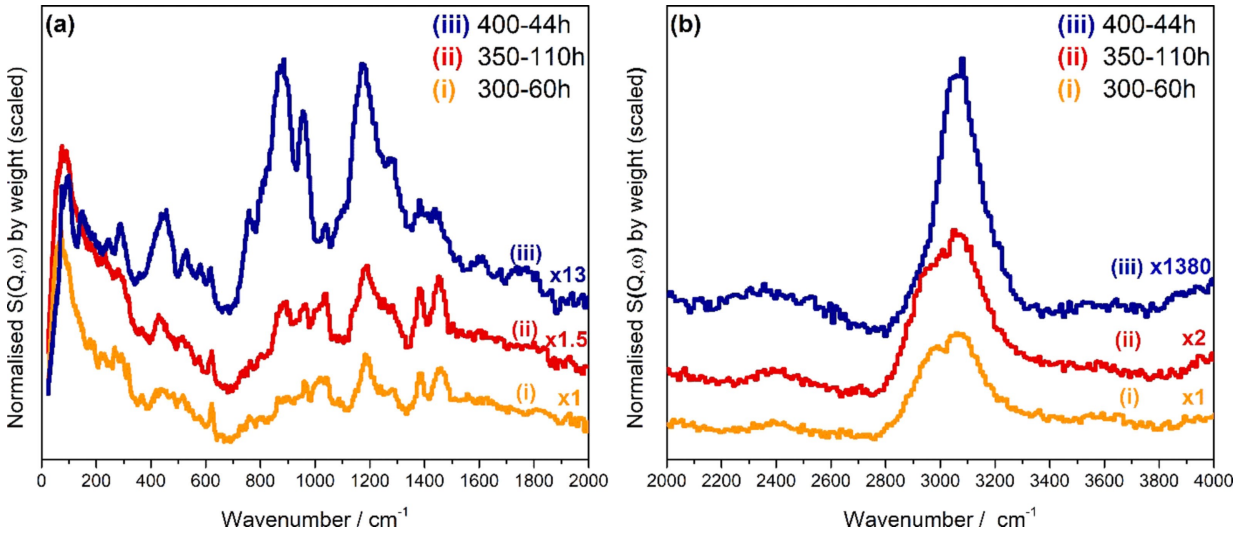

Figure 4. INS spectra of the MTH reacted ZSM-5: (i) 300°C for 60 h; (ii) 350°C for 110 h; (iii) 400°C for 44 h. The spectra are normalised to sample mass and scaled by the factors shown. (a) Spectra collected using the TOSCA spectrometer;[37,53,54] (b) spectra collected with the MAPS spectrometer at an incident energy of 5244 cm^{-1} using the A-chopper package.[37,55]

Figure 4(b) presents the spectra in the C–H stretching region of the spectrum and indicates the reaction temperature to affect the distribution of sp^3 hybridized C–H modes (*i.e.*, aliphatic C–H) and sp^2 hybridized C–H modes (*i.e.*, olefinic and/or aromatic C–H). INS spectroscopy is a quantitative technique, where the scattering intensity is proportional to the number of oscillators and the amplitude of motion that the hydrogen experiences within a specific mode.[37,38] This means that curve fitting can be used to determine the ratio of aliphatic: olefinic/aromatic C–H modes for any given spectrum. Figures S7–S9 present curve fitting outcomes for the spectra shown in Figure 4(b).

The ratio of sp^3 : sp^2 ν(C–H) modes for the 300 °C sample is 1: 1.35, which decreases to 1: 1.14 for the 350 °C sample. The sp^3 hybridized ν(C–H) signal is absent in the case of the 400 °C sample (Figure 4(b)(iii)). Thus, for the long run samples, increasing temperature leads to a diminution of the aliphatic component of the HCP. Moreover, the scaling factors in Figure 4(b) reveal a further facet of the modifications within the HCP as a function of temperature and T-o-S. Namely, the quasi-deactivated sample contains significantly less hydrogen than that seen for steady-state operation, as represented by the spectrum of the 350 °C sample (Figure 4(b)(ii)). Collectively, Figure 4(b) signifies the presence of a dehydrogenation pathway within the hydrocarbon pool as the catalyst evolves towards a deactivation regime. Indeed, the spectrum of the 400–44 h sample closely resembles that of amorphous carbon, with hydrogen termination of the graphene planes.[58,59] The low energy spectra (Figure 4a) are consistent with this deduction (see discussion of Figure 6 below).

Recent work by Zachariou *et al.* has reported on the INS spectra of a series of unsaturated hydrocarbons, with an emphasis on the methyl torsion mode.[45] The molecules examined, cyclic and polycyclic unsaturated compounds (including all 12 methylated benzenes), constitute candidate molecules that could contribute to the HCP. Here, we use that study to work towards an assignment of the spectra presented in Figure 4. Synthetic spectra were generated by adding spectra of the model compounds in an equimolar ratio; similar hydrocarbons were added together in order to highlight common spectral features. This is only possible because of the quantitative nature of the INS technique. The results of this process are shown in Figure 5, where the simulated spectra are compared to the spectrum for the long-run steady-state sample (350–110 h, Figure 4(a)(ii)).

A doublet of peaks at 1354 cm^{-1} and 1458 cm^{-1} are evident in all plots in Figure 4(a), with reference to Figure 5(a) they are assigned to symmetric and asymmetric CH_3 bending modes of highly methylated benzenes (≥4 methyl groups).[45] The same doublet is also seen in methylated polycyclic aromatics (Figure 5(b)), therefore some of the intensity could correspond to those hydrocarbons as well. Peaks about 1200 cm^{-1} are observed in the simulated spectra of polycyclic molecules (Figure 5(b)) but these features are absent in the spectra of

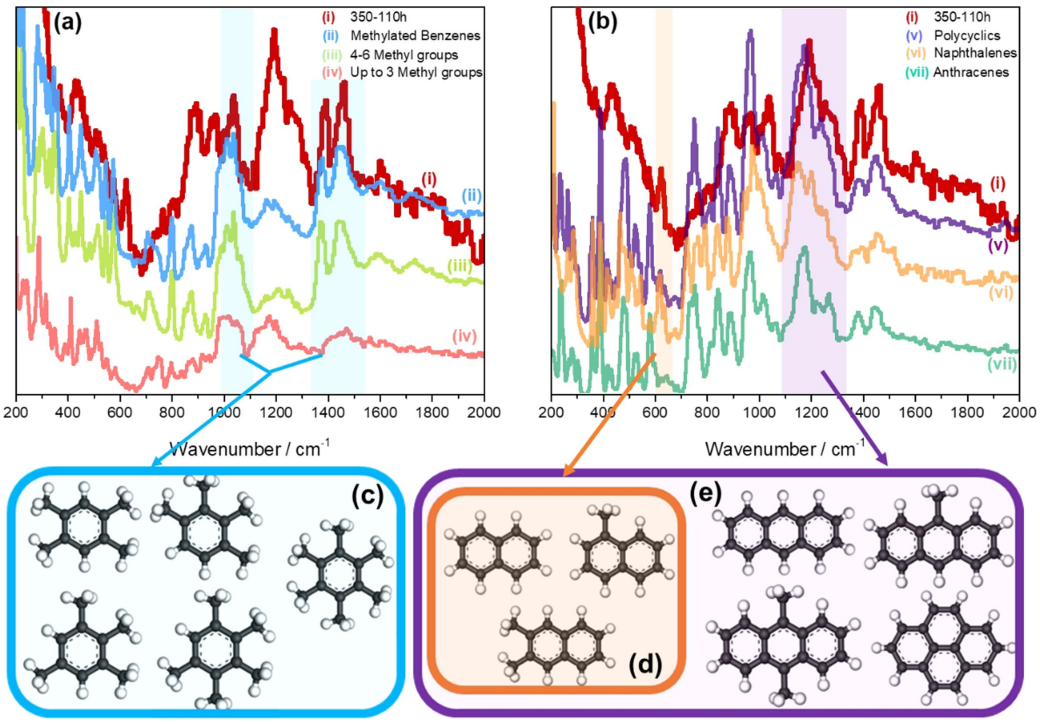

Figure 5. Experimental 350–110 h spectrum **(i)** compared with the generated addition spectra (equimolar additions of model compound spectra). The colour coding highlights regions which are characteristic of the different hydrocarbons. **(a)** Comparison with methylated benzenes: **(ii)** all of the methylated benzenes; **(iii)** methylated benzenes with more than 4 substitutions; **(iv)** methylated benzenes with up to 3 methyl substitutions. **(b)** Comparison with polycyclic aromatic molecules: **(v)** all polycyclics, **(vi)** naphthalenes and **(vii)** anthracenes. Sections (c)-(d) illustrate the principal contributors to the spectra: **(c)** methylated benzenes with ≥4 methyl groups; **(d)** naphthalenes; **(e)** anthracenes and pyrene. For an expanded version of this figure see ESI (S10, S11).

methylated benzenes (Figure 5(a)). On this basis, the strong peak at 1200 cm^{-1} with a high energy shoulder at 1246 cm^{-1} is assigned to C–H bending modes of polycyclic aromatic molecules, such as naphthalene.[60,61] When inspecting the ratio of the 1200 cm^{-1} peak with other peaks in the reference compounds, it is seen that for all the polycyclic hydrocarbons it has approximately the same intensity as the peak found at 910 cm^{-1} that corresponds to a CH wag.[60] However, in the steady-state MTH spectrum (Figure 5) the relative intensity of the two peaks (1200 cm^{-1} and 910 cm^{-1}) is different, with the 1200 cm^{-1} peak being significantly more intense. This suggests that there is an additional species that is also contributing to the intensity of the 1200 cm^{-1} peak. We will return to this point later.

In the MTH spectrum (Figure 5(i)) a sharp band is located at 600 cm^{-1}. This band is only present in the spectra of naphthalene model compounds and, consequently, it is assigned to the double aromatic ring distortion of naphthalenes.[61] The broad peaks below 400 cm^{-1} are largely attributed to the methyl torsions of the methylated benzenes and the polycyclic species.[45] We have shown elsewhere that the degree of methyl substitution on the aromatic rings and the local environment both strongly influence the methyl torsion transition energies.[45] This helps explain why there are no distinct methyl torsion peaks present in the HCP spectrum (Figure 5(i)).

As discussed above, the spectrum for the long-run 400 °C sample (400–44 h, Figure 4) is representative of a sample approaching deactivation. Interestingly, the INS spectrum closely matches that reported for activated carbon and glassy carbon.[58] To illustrate this point, Figure 6 plots the INS spectrum of the quasi-deactivated HCP alongside that of reference spectra for graphite[59] and glassy carbon.[58] The graphite spectrum (Figure 6(iii)) does not share any of the spectral features with the 400–44 h sample, whereas the glassy carbon (Figure 6(ii)) provides a close match. This outcome suggests that the coke that forms on the surface of the zeolite as the catalyst displays deactivation characteristics (Figure 1) is irregular and closer to glassy carbon than structured graphite. Glassy carbon is a type of amorphous carbon with no long-range crystalline order.[62,63] The major peak at ~880 cm^{-1} is indicative of isolated hydrogen atoms at carbon edge termination points.[58] It is presumed that a phase of the HCP evolution involves polycyclic aromatics continuing to grow within the zeolite pores until they reach another set, which leads to termination. Chua and Stair suggested from UV-Raman spectroscopy that the amorphous carbon present is not 2 dimensional but rather closer to a chain-like topology.[15] This agrees with the INS observation of the amorphous carbon being similar to glassy carbon in structure and looking nothing like graphite. The doublet at 1354 cm^{-1} and 1458 cm^{-1} is still present in the 400–44 h spectrum. This suggests that the HCP pool products are still present, but at a much lower degree, as the spectrum is dominated by amorphous carbon. The presence of amorphous carbon also explains the anomalous intensity of the 1200 cm^{-1} peak in the spectra of the 300 and 350 °C samples, showing that coke is already present in a working, steady-state catalyst. This is not however the dominant form of deactivation in those samples as seen from the TPO data (Figure S4) and the higher visibility of the HCP peaks. This is consistent with the literature that suggests that at lower temperatures the dominant deactivation pathway is caused by the build-up of methylated polycyclic aromatic molecules

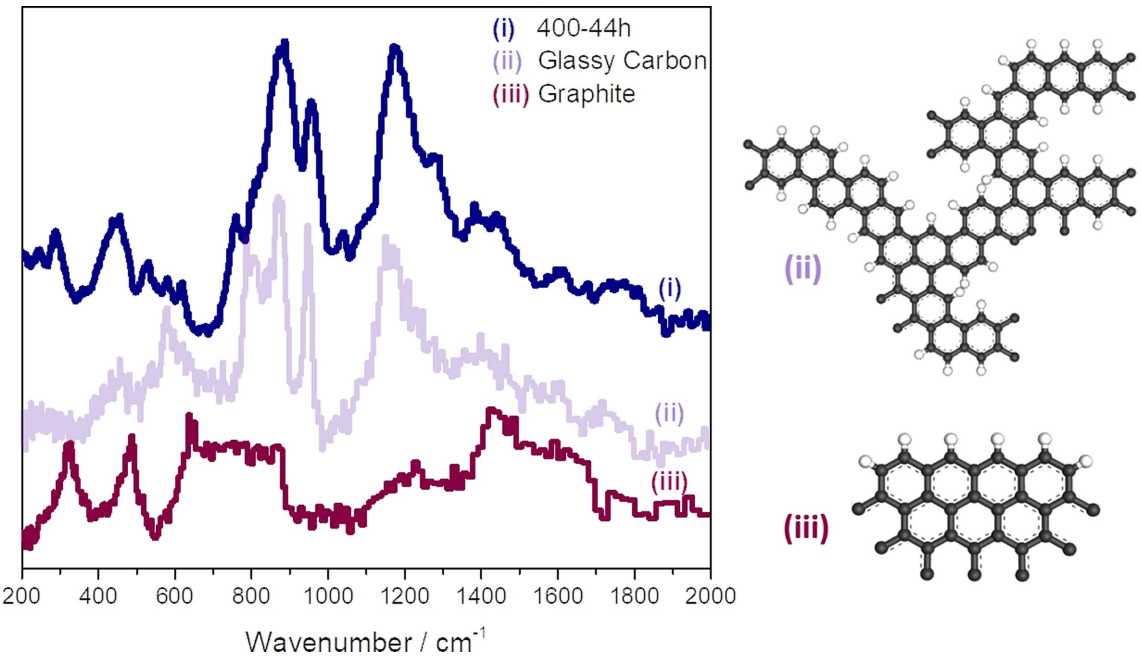

Figure 6. Experimental 400–44 h spectrum **(i)** compared with model compounds: **(ii)** glassy carbon;[58] **(iii)** graphite[59] (Glassy carbon and graphite molecule schematics are a schematic representation and not specific molecular models).

within the pores. At higher temperatures, the major pathway of deactivation is pore blockage by external coke.[18,19,41,43]

The presence of coke also explains the apparent contradiction that on increasing T-o-S the degree of methylation increases (see catch-pot analysis, Figure S3), which requires the presence of sp^3 hybridised ν(C–H), but the ratio of sp^3:sp^2 C–H decreases with time (Section 2.2), *i.e.*, the processes of ring methylation and dehydrogenation are occurring in parallel.

^{13}C solid-state NMR spectroscopy

The ^{13}C ss-NMR spectra of the post-reaction samples support the INS assignments. Cross-polarised spectra measured after even short reaction times (Figure S12) showed signatures of aromatic carbons (~130 ppm with strong spinning side bands) and methyl groups (~20 ppm), with the contribution of aromatic signals increasing at longer reaction times (Figure S13). To quantify the carbon signals, spectra from an active (350–110 h) and quasi-deactivated (400–44 h) catalyst were measured with a quantitative 90–180° Hahn-Echo pulse sequence with 1 rotor delay and high spinning speed.[64] The spectra are presented in Figure 7, with significant differences between samples apparent, indicating differences in the nature of the 'coke' formed in each case. The peak at 20.8 ppm in the 350–110 h spectrum has disappeared in the 400–44 h spectrum, whereas the peak at 129.2 ppm has upshifted to 126.3 ppm. The 20.8 ppm peak is assigned to the aliphatic carbon of the methyl carbons of methylated aromatic compounds.[56,65] The shoulders present at 16.6 ppm and 13.5 ppm are associated with polymethyl substitutions on aromatic compounds.[65] Both peaks at 129.2 ppm and 126.3 ppm are typical of aromatic carbons, both being close in chemical shift to that of methylated benzenes and polycyclic aromatic molecules,[66,67] and both spectra contain strong spinning side bands (marked *) due to the anisotropic chemical shift of the aromatic species present. Although it is not possible to assign the peaks to a particular hydrocarbon, both peaks in the two samples are broad with a range of shoulders suggesting different levels of methyl substitution. The quasi-deactivated catalyst contains many fewer methyl groups than the active catalyst, consistent with the INS spectra.

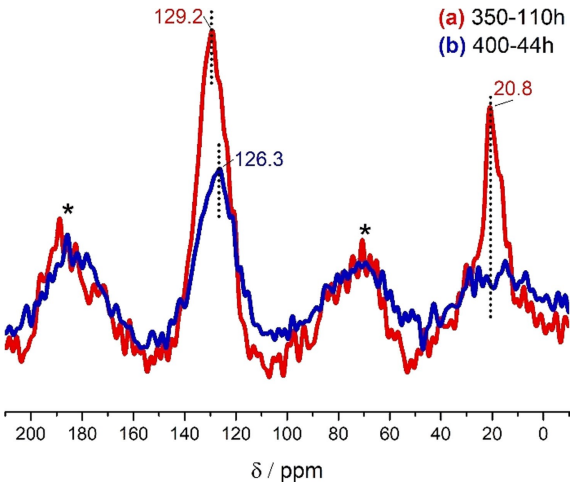

Figure 7. ^{13}C-ssNMR spectra of the reacted ZSM-5 samples of (a) 350 °C–110 h (red) and (b) 400 °C–44 h (blue) collected at a spinning speed of 10 KHz (* spinning side bands).

For this pulse sequence, the integrated intensity is directly proportional to the number of carbon atoms present,[64] and Figure 7 shows the 400–44 h spectrum to possess less carbon than the 350–110 h sample. This outcome contrasts with the TPO analysis (Table 1) that indicates an opposite trend. This apparent contradiction is understood in terms of graphitic carbon and amorphous coke being NMR invisible;[67] therefore, these species are unable to contribute to the carbon intensity in Figure 7. An increasing fraction of NMR invisible carbon with increasing coke content was also observed by Meinhold and Bibby.[65] Thus, the ^{13}C NMR measurements are supportive of the INS-derived concept of the evolving nature of the HCP, which is influenced by temperature and time. The Supporting Information section includes a series of ancillary analytical measurements of the post-reaction samples – temperature-programmed oxidation (Figures S4, S5), ^{27}Al ss-NMR (Figures S14) and ^{29}Si ss-NMR (Figures S15, S16) – all of which are consistent with the proposed dynamical form of the HCP outlined above.

Conclusion

INS spectroscopy has been used as the principal probe to interrogate the ZSM-5/MTH reaction system, with an emphasis on the form of the hydrocarbon pool. Reactions in the temperature range 300–400 °C were studied at short (2 h) and extended (t ≥ 44 h) time domains. The following conclusions have been drawn.

- At short reaction times the INS spectra indicate a mixture of hydrocarbons to be present but with no singular molecular entity dominant (Figure S6).
- The INS spectra for longer run samples recorded at 300 and 350 °C exhibit the same spectral pattern as previously reported (Figure 4) and may be characterised as the vibrational fingerprint of the working hydrocarbon pool (HCP). Assignment of the vibrational spectrum reveals this variant of the HCP to comprise polycyclic aromatics, poly-methylated benzenes and amorphous coke (Figure 5). The INS analysis on these larger scale working catalysts is validated by comparison with other spectroscopies. The amorphous coke present is at much lower quantities at these two temperatures, suggesting that any degree of deactivation being observed (drop in methanol conversion) to be due to pore filling rather than pore blockage from external coke. Polycyclic aromatics and polymethylated benzenes are found to be the dominant species within the HCP at this stage of the catalytic lifetime, in agreement with the literature, despite the increased sample size required for the INS samples.
- The reaction profile of the longer run, higher temperature sample indicates the catalyst to be approaching a deactivation regime (Figure 1). The INS spectrum of this sample is

distinct and noticeably different to the catalyst operating under steady-state conditions (Figure 4). The spectrum closely corresponds to that of glassy carbon (Figure 6), a form of amorphous carbon with no long-range crystalline order and isolated hydrogen atoms at carbon edge termination points. This moiety is the dominant species, although residual traces of the HCP are also present. This suggests that the degree of deactivation being observed is due to external pore blocking and not due to pore filling or because of loss of acid sites. The shift in the sp^3:sp^2 ratio of the high energy INS spectra suggests that the proportion of the HCP present is relatively small in comparison with the amorphous coke build-up. This is demonstrated by their being no detectable sp^3 C–H present. The small contribution from the HCP observed in the lower energy 400–44 h sample could still be there, but masked by the heavy contribution of sp^2 C–H.

- The intensity of the 400–44 h sample in comparison with the 300 and 350 °C sample spectra must also be acknowledged. There is a large intensity difference between them, with a large loss of INS intensity being observed in the 400–44 h sample. This suggests a large degree of dehydrogenation and carbon retention at higher temperatures.

The INS spectra provide molecular information over the complete vibrational frequency range on the form of the HCP during (i) its evolutionary phase, (ii) steady-state operation and (iii) a quasi-deactivation phase. TPO, DRIFTS and ^{13}C solid-state NMR spectroscopic measurements are consistent with the INS-derived findings. The increased sample sized required for the INS measurements does not show any difference in the HCP build up or on the temperature dependent pathways of deactivation compared with the microsampling of other spectroscopic methods. The INS technique is particularly powerful for observing the deactivation stage of MTH catalysis.

We point out also the future possibilities of quantifying the different species with INS following successful assignment of the spectra.

Acknowledgements

Johnson Matthey plc. is thanked for supplying the ZSM-5 zeolite and for financial support through the provision of industrial CASE studentships in partnership with the EPSRC (APH (EP/P510506/1), AZ (EP/N509176/1)). Experiments at the ISIS Neutron and Muon Source were made possible by a beam time allocation from the Science and Technologies Facilities Council.[68] The resources and support provided by the UK Catalysis Hub via *membership of the UK Catalysis Hub consortium and funded by EPSRC grants EP/R026815/1 and EP/R026939/1 are gratefully acknowledged. This research has been performed with the use of facilities and equipment at the Research Complex at Harwell; the authors are grateful to the Research Complex for this access and support. Dr Andrea Sauerwein and Dr Jonathan Bradley (Johnson Matthey) are thanked for their help in acquiring the ^{29}Si and ^{27}Al NMR spectra using the Bruker Avance Neo spectrometer.*

Conflict of Interest

The authors declare no conflict of interest.

Keywords: HZSM-5 · Methanol-to-Hydrocarbons · Hydrocarbon Pool · Deactivation · Inelastic Neutron Scattering · Solid-State NMR Spectroscopy

[1] I. Yarulina, A. D. Chowdhury, F. Meirer, B. M. Weckhuysen, J. Gascon, *Nat. Cat.* **2018**, *1*, 398–411.
[2] U. Olsbye, S. Svelle, K. P. Lillerud, H. Wei, Y. Y. Chen, J. F. Li, J. G. Wang, W. B. Fan, *Chem. Soc. Rev.* **2015**, *44*, 7155–7176.
[3] H. Schulz, *Catal. Lett.* **2018**, *148*, 1263–1280.
[4] S. Xu, Y. Zhi, J. Han, W. Zhang, X. Wu, T. Sun, Y. Wei, Z. Liu, *Adv. Catal.* **2017**, *61*, 37–122.
[5] K. Hemelsoet, J. Van Der Mynsbrugge, K. De Wispelaere, M. Waroquier, V. Van Speybroeck, *ChemPhysChem* **2013**, *14*, 1526–1545.
[6] J. L. White, *Catal. Sci. Technol.* **2011**, *1*, 1630–1635.
[7] T. R. Forester, S. Wong, R. F. Howe, *J. Chem. Soc. Chem. Commun.* **1986**, *21*, 1611–1613.
[8] T. R. Forester, R. F. Howe, *J. Am. Chem. Soc.* **1987**, *109*, 5076–5082.
[9] H. Yamazaki, H. Shima, H. Imai, T. Yokoi, T. Tatsumi, J. N. Kondo, *J. Phys. Chem. C* **2012**, *116*, 24091–24097.
[10] H. Yamazaki, H. Shima, H. Imai, T. Yokoi, T. Tatsumi, J. N. Kondo, *Angew. Chem. Int. Ed.* **2011**, *50*, 1853–1856; *Angew. Chem.* **2011**, *123*, 1893–1896.
[11] Y. Ono, T. Mori, *J. Chem. Soc. Faraday Trans. 1* **1981**,*77*, 2209–2221.
[12] I. B. Minova, S. K. Matam, A. Greenaway, C. R. A. Catlow, M. D. Frogley, G. Cinque, P. A. Wright, R. F. Howe, *ACS Catal.* **2019**, *9*, 6564–6570.
[13] J. Won Park, G. Seo, *Appl. Catal. A* **2009**, *356*,180–188.
[14] E. D. Hernandez, F. C. Jentoft, *ACS Catal.* **2020**, *10*, 5764–5782.
[15] Y. T. Chua, P. Stair, *J. Catal.* **2003**, *213*, 39–46.
[16] M. Signorile, D. Rojo-Gama, F. Bonino, P. Beato, S. Svelle, S. Bordiga, *Phys. Chem. Chem. Phys.* **2018**, *20*, 26580–26590.
[17] I. Lezcano-González, E. Campbell, A. E. J. Hoffman, M. Bocus, I. V. Sazanovich, M. Towrie, M. Agote-Aran, E. K. Gibson, A. Greenaway, K. De Wispelaere, V. Van Speybroeck, A. M. Beale, *Nat. Mater.* **2020**, *19*, 1081–1087.
[18] E. Borodina, F. Meirer, I. Lezcano-Gonzáles, M. Mokhtar, A. M. Asiri, S. A. Al-Thabaiti, S. N. Basahel, J. Ruiz-Martinez, B. M. Weckhuysen, *ACS Catal.* **2014**, *5*, 992–1003.
[19] D. Mores, E. Stavitski, M. H. Kox, J. Kornatowski, U. Olsbye, B. M. Weckhuysen, *Chem. Eur. J.* **2008**, *14*, 11320–11327.
[20] E. Borodina, H. Sharbini Harun Kamaluddin, F. Meirer, M. Mokhtar, A. M. Asiri, S. A. Al-Thabaiti, S. N. Basahel, J. Ruiz-Martinez, B. M. Weckhuysen, *ACS Catal.* **2017**, *7*, 5268–52.
[21] D. Fu, O. van der Heijden, K. Stanciakova, J. E. Schmidt, B. M. Weckhuysen, *Angew. Chem. Int. Ed.* **2020**, *59*, 15502–15506.
[22] Y. Shen, T. T. Le, D. Fu, J. E. Schmidt, M. Filez, B. M. Weckhuysen, J. D. Rimer, *ACS Catal.* **2018**, *8*, 11042–11053.
[23] J. Goetze, B. M. Weckhuysen, *Catal. Sci. Technol.* **2018**, *8*, 1632–1644.
[24] E. C. Nordvang, E. Borodina, J. Ruiz-Martinez, R. Fehrmann, B. M. Weckhuysen, *Chem. Eur. J.* **2015**, *21*, 17324–17335.
[25] W. Dai, C. Wang, M. Dyballa, G. Wu, N. Guan, L. Li, Z. Xie, M. Hunger, *ACS Catal.* **2015**, *5*, 317–326.
[26] Y. Jiang, J. Huang, V. R. Reddy Marthala, Y. S. Ooi, J. Weitkamp, M. Hunger, *Microporous Mesoporous Mater.* **2007**, *105*, 132–139.
[27] M. J. Wulfers, F. C. Jentoft, *ACS Catal.* **2014**, *4*, 3521–3532.
[28] J. F. Haw, J. B. Nicholas, W. Song, F. Deng, Z. Wang, T. Xu, C. S. Heneghan, *J. Am. Chem. Soc.* **2000**, *122*, 4763–4775.
[29] J. F. Haw, W. Song, D. M. Marcus, J. B. Nicholas, *Acc. Chem. Res.* **2003**, *36*, 317–326.
[30] W. Wang, A. Buchholz, M. Seiler, M. Hunger, *J. Am. Chem. Soc.* **2003**, *125*, 15260–15267.
[31] C. Wang, Y. Chu, A. Zheng, J. Xu, Q. Wan, P. Gao, G. Qi, Y. Gong, F. Deng, *Chem. Eur. J.* **2014**, *20*, 12432–12443.
[32] C. Wang, J. Xu, F. Deng, *ChemCatChem* **2020**, *12*, 965–980.
[33] X. Wu, S. Xu, W. Zhang, J. Huang, J. Li, B. Yu, Y. Wei, Z. Liu*, *Angew. Chem. Int. Ed.* **2017**, *56*, 9039–9043; *Angew. Chem.* **2017**, *129*, 9167–9171.

[34] D. Fu, A. Lucini-Paioni, C. Lian, O. van der Heijden, M. Baldus, B. M. Weckhuysen, *Angew. Chem. Int. Ed.* **2020**, *59*, 20024–20030.
[35] W. Dai, C. Wang, M. Dyballa, G. Wu, N. Guan, L. Li, Z. Xie, M. Hunger, *ACS Catal.* **2015**, ***5***, 317–326.
[36] X. Wu, S. Xu, Y. Wei, W. Zhang, J. Huang, S. Xu, Y. He, S. Lin, T. Sun, Z. Liu, *ACS Catal.* **2018**, *8*, 7356–7361.
[37] S. F. Parker, D. Lennon, P. W. Albers, *Appl. Spectrosc.* **2011**, *165*, 1325–1341.
[38] P. C. H. Mitchell, S. F. Parker, A. J. Ramirez-Cuesta, A. J. J. Tomkinson, *Mater. Sci. Catal. World Sci.* **2005**, *642*.
[39] A. Zachariou, A. P. Hawkins, S. F. Parker, D. Lennon, R. F. Howe, *Catal. Today*. **2020**, *368*, 20-27 .
[40] M. D. Argyle, C. H. Bartholomew, *Catalysts* **2015**, *5*, 145–269.
[41] H. Schulz, *Catal. Today* **2010**, *154*, 183–194.
[42] B. A. Sexton, A. E. Hughes, D. M. Bibby, *J. Catal.* **1988**, *109*, 126–131.
[43] D. Mores, J. Kornatowski, U. Olsbye, B. M. Weckhuysen, *Chem. Eur. J.* **2011**, *17*, 2874–2884.
[44] C. D. Chang, *Catal. Rev.* **1983**, *25*, 1–118.
[45] A. Zachariou, A. P. Hawkins, P. Collier, R. F. Howe, D. Lennon, S. F. Parker, *ACS Omega* **2020**, *5*, 2755–2765.
[46] R. Warringham, D. Bellaire, S. F. Parker J Taylor, R. A. Ewings, C. M. Goodway, M. Kibble, S. R. Wakefield, M. Jura, M. P. Dudman, R. P. Tooze, P. B. Webb, D. Lennon, *J. Phys. Conf. Ser.* **2014**, *554*.
[47] Suwardiyanto, R. F. Howe, E. K. Gibson, C. R. A. Catlow, A. Hameed, J. McGregor, P. Collier, S. F. Parker, D. Lennon, *Faraday Discuss.* **2017**, *197*, 447–472.
[48] R. F. Howe, J. McGregor, S. F. Parker, P. Collier, D. Lennon, *Catal. Lett.* **2016**, *146*, 1242–1248.
[49] S. Müller S, Y. Liu, M. Vishnuvarthan, X. Sun, A. C. van Veen, G. L. Haller, M. Sanchez-Sanchez, J. A. Lercher, *J. Catal.* **2015**, *325*, 48–59.
[50] D. M. Bibby, N. B. Milestone, J. E. Patterson, L. P. Aldridge, *J. Catal.* **1986**, *97*, 493–502.
[51] P. A. Jacobs, R. von Ballmoos, *J. Phys. Chem.* **1982**, *86*, 3050–3052.
[52] L. Kubelková, J. Nováková, K. Nedomová, *J. Catal.* **1990**, *124*, 441–450.
[53] D. Colognesi, M. Celli, F. Cilloco, R. J. Newport, S. F. Parker, V. Rossi-Albertini, F. Sacchetti, J. Tomkinson, M. Zoppi, *Appl. Phys. A.* **2002**, *74*, 64–66.
[54] R. S. Pinna, S. Rudić, S. F. Parker, J. Armstrong, M. Zanetti, G. Škoro, S. P. Waller, D. Zacek, C. A. Smith, M. J. Capstick, D. J. McPhail, D. E. Pooley, G. D. Howells, G. Gorini, F. Fernadez-Alonso, *Nucl. Instrum. Methods Phys. Res. Sect. A* **2018**, *896*, 68–74.
[55] Science Technology and Facilities Council. MAPS Instrument. Available at: https://www.isis.stfc.ac.uk/Pages/maps.aspx. (Accessed: 16th April 2020).
[56] A. Zachariou, A. P. Hawkins, D. Lennon, S. F. Parker, Suwardiyanto, S. K. Matam, C. R. A. Catlow, P. Collier, A. Hameed, J. McGregor, R. F. Howe, *Appl. Catal. A Gen.* **2019**, *569*, 1–7.
[57] A. Zachariou, A. P. Hawkins, P. Collier, R. F. Howe, S. F. Parker, D. Lennon, *Top. Catal.* **2020**, *63*, 370–377.
[58] S. F. Parker, S. Imberti, S. K. Callear, P. W. Albers, *Chem. Phys.* **2013**, *427*, 44–48.
[59] J. K. Walters, R. J. Newport, S. F. Parker, W. S. Howells, *J. Phys. Condens. Matter* **1995**, ***7***, 10059–10073.
[60] D. Lin Vien, N. B. Colthup, W. G. Fateley, J. G. Grasselli, *The Handbook of Infrared and Raman Characteristic Frequencies of Organic Molecules*, Academic Press. Analytical Chemistry **1975**.
[61] E. R. Lippincott, E. J. O'Reilly, *J. Chem. Phys.* **1955**, *23*, 238–244.
[62] E. Fitzer, K. H. Kochling, H. P. Boehm, H. Marsh, *IUPAC Pure Appl. Chem.* **1995**, *67*, 473–506.
[63] D. F. Mildner, J. M. Carpenter, *J. Non-Cryst. Solids* **1982**, *47*, 391–402.
[64] J. D. Mao, K. S. Rohr, *Environ. Sci. Technol.* **2004**, *38*, 2680–2684.
[65] R. H. Meinhold, D. M. Bibby, *Zeolites* **1990**, *10*, 121–130.
[66] R. S. Ozubko, G. W. Buchanan, I. C. P. Smith, *Can. J. Chem.* **1974**, *52*, 2493–2501.
[67] K. Barbera, S. Sorensen, S. Bordiga, J. Skibsted, H. Fordsmand, P. Beato, T. V. W. Janssens, *Catal. Sci. Technol.* **2012**, *2*, 1196–1206.
[68] R. Howe, A. Zachariou, A. Hawkins,Suwardiyanto, P. Collier, D. Lennon, S. F. Parker, STFC ISIS Neutron and Muon Source **2018**, doi: 10.5286/ISIS. E.RB1720211.

Manuscript received: February 24, 2021
Accepted manuscript online: March 8, 2021
Version of record online: May 4, 2021